Aerosol-CO relationship and aerosol effect on ice cloud particle size: Analyses from Aura Microwave Limb Sounder and Aqua Moderate Resolution Imaging Spectroradiometer observations

Jonathan H. Jiang,[1] Hui Su,[1] Steven T. Massie,[2] Peter R. Colarco,[3] Mark R. Schoeberl,[3] and Steven Platnick[3]

Received 4 May 2009; revised 29 June 2009; accepted 17 August 2009; published 30 October 2009.

[1] We examine the relation between Aqua Moderate Resolution Imaging Spectroradiometer (MODIS) aerosol optical thickness (AOT) and Aura Microwave Limb Sounder upper tropospheric (UT) carbon monoxide (CO) to address when CO can be used as a proxy for aerosols. Ice cloud effective radii (r_e), also from Aqua MODIS, are also analyzed to investigate possible aerosol effects on ice clouds. Our analysis focuses on five regions where ice clouds are collocated with high UT CO loadings: South America (SAM), southern Africa (SAF), northern Africa (NAF), South Asia (SAS), and East Asia (EAS). We find three levels of AOT to CO sensitivity. High AOT sensitivity to CO is characterized by a rapid increase of AOT when CO increases. SAM in August–November and SAF in June–September fall into this category. Moderate AOT sensitivity to CO is characterized by moderate increase of AOT with CO. It includes SAF in October–May, NAF in January–March, SAS in all months, and EAS in August–September. The other months for each region fall into the low sensitivity category. The variations of sensitivity in different regions and seasons result from different emission sources coupled with dynamic influence. CO can be used as an aerosol proxy for the "high" and "moderate" sensitivity cases. During those times, r_e for polluted clouds is smaller than that for clean clouds, suggesting an indirect effect of aerosol on ice clouds. CO is not a good aerosol index in the low sensitivity cases, in which polluted clouds defined by CO loadings do not show significant differences from clean clouds in r_e.

Citation: Jiang, J. H., H. Su, S. T. Massie, P. R. Colarco, M. R. Schoeberl, and S. Platnick (2009), Aerosol-CO relationship and aerosol effect on ice cloud particle size: Analyses from Aura Microwave Limb Sounder and Aqua Moderate Resolution Imaging Spectroradiometer observations, *J. Geophys. Res.*, *114*, D20207, doi:10.1029/2009JD012421.

1. Introduction

[2] The composition of the atmosphere has undergone dramatic changes in the past few decades due to human activities. The quasi-exponential growth in world population and industrialization has led to rapid increases of aerosols due to fossil fuel, biofuel, as well as biomass burning emissions [e.g., *Crutzen and Andreae*, 1990]. Numerous models have predicted that these aerosols can affect the climate system indirectly by changing cloud properties, such as cloud particle sizes, and therefore affect condensation and evaporation rates, latent heat release, collision coalescence efficiency, cloud reflectance, lifetime, and precipitation [e.g., *Lohmann and Feichter*, 2005; *Penner et al.*, 2006]. However, the accurate quantification of these aerosol effects is still quite uncertain [*Denman et al.*, 2007].

[3] One reason for the large uncertainty of the aerosol indirect effect is that it is extremely difficult to observe aerosols in the presence of clouds. Because clouds and aerosols both scatter light, aerosols cannot be easily detected by satellite sensors when they are inside or near clouds. One way to infer the presence of aerosols inside or near clouds is to use an observable pollutant as a "proxy" for aerosols. The correlation between enhanced aerosols and high carbon monoxide (CO) values has been noted before [e.g., *Kim et al.*, 2004; *Li et al.*, 2005; *Massie et al.*, 2006]. Both CO and aerosols can be produced by incomplete combustion that occurs in biomass burning, power generating plants, or fossil fuel powered automobiles. High values of CO in the upper troposphere (UT) can be associated with pollution (including aerosols) entrained into convective systems [e.g., *Schoeberl et al.*, 2006; *Fu et al.*, 2006; *Li et al.*, 2005]. On the other hand, convective cloud systems that have entrained aerosols from fires/combustion should exhibit high values of CO. *Li et al.* [2005] showed that the CO observed by the Microwave Limb Sounder (MLS) in the UT over the Tibetan plateau area are closely collocated with aerosols simulated by a chemistry transport model. However, such an aerosol proxy should be used with caution. *Jiang et al.* [2007] showed that distribu-

[1]Jet Propulsion Laboratory, California Institute of Technology, Pasadena, California, USA.
[2]National Center for Atmospheric Research, Boulder, Colorado, USA.
[3]NASA Goddard Space Flight Center, Greenbelt, Maryland, USA.

Copyright 2009 by the American Geophysical Union.
0148-0227/09/2009JD012421

Table 1. Criteria Used to Define "Clean" and "Polluted" Clouds and "AOT Sensitivities to CO" Categories[a]

Separating Clean and Polluted Clouds		AOT Sensitivity to CO		
Clean (ppbv)	Polluted (ppbv)	High	Moderate	Low
CO $\leq$ 100–110	CO $\geq$ 220–240	$\delta > 0.2$	$\delta \sim 0.1$–0.2	$\delta < 0.1$

[a]The AOT sensitivity to CO is defined by value of δ, which is the difference of MODIS AOT in the clean and polluted environments as indicated by the collocated MLS CO.

tion and variation of UT CO do not solely depend on the aerosol emission source but also depend on the environmental conditions such as convective strength and large-scale winds. Also, aerosols are subject to removal processes such as wet and dry deposition while CO is not subject to these processes. Furthermore, CO has a longer lifetime (~2 months) than aerosols (about a week). Hence, when and where CO can be used as a proxy for aerosols requires careful analysis.

[4] *Jiang et al.* [2008] found a positive correlation between MLS CO and Moderate Resolution Imaging Spectroradiometer (MODIS) aerosol optical thickness (AOT) during the dry season (June–October) in South America. Using the MLS CO as a proxy for aerosol in cloudy regions, *Jiang et al.* [2008] demonstrated that for the same ice water content (IWC) amount, the polluted clouds have smaller effective radii and are associated with weaker precipitation rates. However, the CO-polluted clouds do not have significantly smaller ice particles than the clean clouds during the wet season (November–May) in South America, when the aerosol wet removal processes by frequent rainfall may be dominant. Note that MODIS AOT used by *Jiang et al.* [2008] and other studies [e.g., *Lin et al.*, 2006] is a columnar quantity without the information of the height of aerosols, which may be located below the clouds. However, when clouds are formed through convection above a region of aerosol pollution, aerosols can reduce cloud particle sizes near cloud base. Smaller liquid particles can then be lofted above the freezing level to form ice clouds that bear the signature of aerosol indirect effects [e.g., *Sherwood*, 2002]. Thus relating UT CO to columnar AOT is reasonable for studies of aerosol effects on ice clouds.

[5] In this study we examine the AOT-CO relations in different regions around the globe in different seasons. We also investigate the aerosol influence on ice cloud particle sizes in these different regions and seasons. Section 2 describes the data sets used for the analyses. Section 3 discusses the regional and seasonal variations of the relationships between CO and AOT. Section 4 discusses ice cloud effective radius (r_e) for polluted and clean clouds as defined by CO loadings. Section 5 presents globally (50°S–50°N) averaged relations among AOT, CO, and r_e. Conclusions and discussion are given in Section 6.

2. Data

2.1. Aura MLS CO and IWC

[6] We use Aura MLS level 2 CO and IWC measurements (version 2.2) from August 2004 to July 2008. The MLS CO and IWC products are described by *Livesey et al.* [2008] and *Wu et al.* [2008], respectively. The lowest usable MLS version 2.2 retrieval level for CO and IWC is 215 hPa (~11 km). The along-track horizontal resolution is about 300 km for IWC and ~400 km for CO, and the vertical resolution is about 4 km for IWC and 5 km for CO. The estimated single measurement precisions are ~20% for CO and ~1 mg/m^3 for IWC. There is a known factor of 2 high bias in the MLS CO data at 215 hPa, but the morphology of CO has been validated to be realistic [*Livesey et al.*, 2008]. Since this study focuses on the correlation between CO and AOT, rather than the absolute values, the high CO bias does not affect our analysis results.

2.2. Aqua MODIS AOT and r_e

[7] The AOT daily data used in this study are Aqua MODIS level 2 aerosol product data (MYD04). The accuracy of AOT is approximately 0.03 over ocean and 0.05 over land [*Remer et al.*, 2005]. The AOT data are specified on 1° latitude by 1.25° longitude grids.

[8] Aqua MODIS r_e is obtained from the collection 005 Level-3 MOD08-D3 product [*Platnick et al.*, 2003]. The Level-3 MOD08-D3 data are generated by subsampling every fifth pixel of the 1 km Level-2 swath product (MYD06). The data are gridded at a 1° × 1° resolution. For ice clouds, the r_e uncertainty is typically about 10%, but it can be variable depending on the corresponding cloud optical thickness and solar viewing geometry. The valid retrieval range for ice cloud r_e is 5–90 μm.

2.3. Data Collocation

[9] The MODIS AOT and r_e are collocated with MLS data by averaging the data in boxes of 3° along the track and 1° across the track centered on the MLS measurement locations (approximately matching the MLS footprints). Such box-averaged sampling collocates MODIS data with the MLS measurements and also increases the amount of useful AOT data, especially in cloudy regions, compared to the linear geographical interpolation used by *Jiang et al.* [2008]. The AOT observations are usually missing in the cloudy regions. Since the MODIS measurements have much higher horizontal resolution, we found that within the 3° × 1° MLS field-of-view boxes, the AOT data are available in about 40% of the areas in which MLS detects clouds. However, the number of samples for in-cloud CO is more than twice of that for box-averaged AOT.

3. Relationships Between AOT and CO for Various Regions and Seasons

[10] To select regions of interest, we classify global ice clouds as clean or polluted by CO loadings, and identify the regions that polluted clouds are predominant. As in the work of *Jiang et al.* [2008], we define "clean clouds" as the clouds where the collocated 215 hPa CO is less than 100–110 ppbv, while the "polluted clouds" are those associated with a high 215 hPa CO loading of >220 to 240 ppbv (Table 1). The slightly different thresholds were chosen (for different regions and seasons discussed later in this section) in order to ensure sufficient samples for either polluted or clean clouds and a clear separation between the clean and polluted cases. We use such CO-defined polluted clouds throughout the text, even though this definition may not be always associated with aerosol pollution as wet and dry deposition can reduce AOT while CO is unaffected.

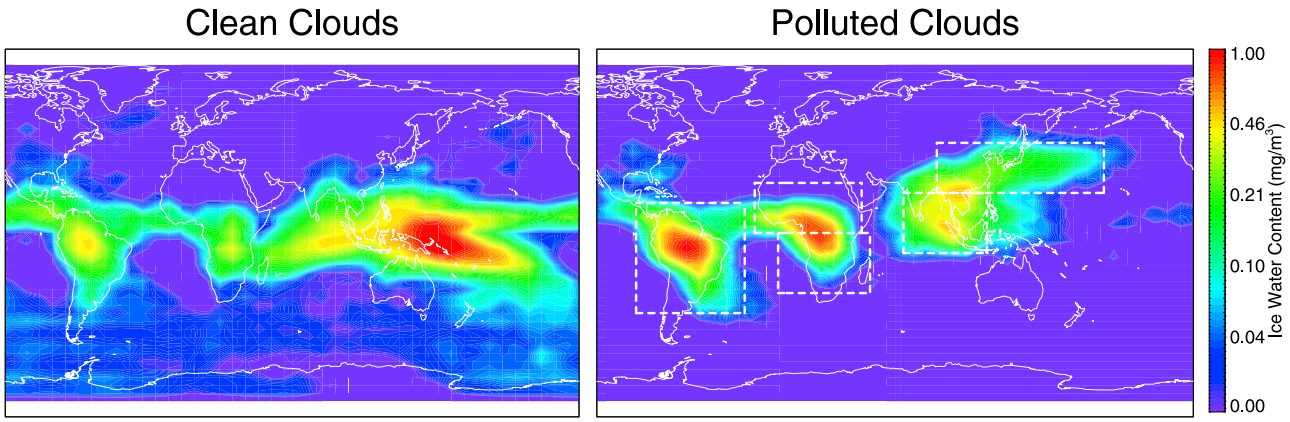

Figure 1. Aura MLS–observed global distributions of clean and polluted clouds IWC at 215 hPa averaged from August 2004 to July 2008. Polluted clouds correspond to collocated MLS CO ≥240 ppbv, and clean clouds correspond to CO ≤100 ppbv.

[11] Figure 1 shows the global distribution of clean and polluted clouds at 215 hPa. The polluted clouds mostly appear over South America, Africa, and Asia, while the clean ice clouds exist mainly over the western Pacific Ocean. We divide the polluted cloudy regions into five subregions based on the different regimes of surface emission or dynamics, namely, South America (SAM), southern Africa (SAF), northern Africa (NAF), South Asia (SAS), and East Asia (EAS).

[12] The AOT-CO relations are analyzed in detail for each region in each month. We define three categories of AOT sensitivity to CO (see Table 1): "high AOT sensitivity to CO" (shortened as "high CO sensitivity"), "moderate AOT sensitivity to CO" (shortened as "moderate CO sensitivity"), and "low AOT sensitivity to CO" (shortened as "low CO sensitivity"). The grouping is based on the difference of AOT for CO-polluted and clean clouds. For the high CO sensitivity category, AOT increases with CO sharply, and the difference between mean AOT for the polluted clouds and clean clouds is greater than 0.2; for the moderate CO sensitivity category, a moderate increase of AOT with CO is observed, in which the AOT differences for the polluted and clean clouds are within 0.1 and 0.2; for the low CO sensitivity case, the mean AOT difference is less than 0.1 for the polluted and clean clouds.

3.1. South America

[13] South America (SAM) biomass burning emissions are responsible for the emission of ~30 Tg/yr of aerosol pollutants to the atmosphere [*Andreae*, 1991]. The biomass burning in the South American continent is characterized by forest fires in the Amazon and anthropogenic vegetation fires in central Brazil throughout the year. These burnings usually intensify during the cold dry season, which starts in June and peaks in September. The burnings weaken when the rainy season begins in November. Figure 2 shows MODIS AOT binned according to the collocated CO values for cloudy (IWC ≥2 mg/m^3) regions in SAM for 12 calendar months (thin lines). Overall, AOT increases as CO increases, but the rate of change of AOT with CO varies from month to month. The monthly AOT sensitivity to CO can be grouped into two categories: one is the high CO sensitivity period from August to November, and another is the low CO sensitivity period from December to July. For the high CO sensitivity period, AOT increases with CO sharply when CO is greater than ~200 ppbv and the difference between mean AOT for the polluted clouds and for the clean clouds is greater than 0.2. It is not surprising that AOT stays flat when CO is around the background value of 100–200 ppbv. For the low CO sensitivity period, the mean AOT difference is less than 0.1 for the polluted and clean clouds. The mean AOT changes averaged over all months for the high and low CO sensitivity periods are shown in thick red and gray lines, respectively. The two periods correspond to the dry biomass burning period and the wet rainy period, respectively. Biomass burning reaches its maximum during September each year. November is a transition month from the dry to wet period. We find that grouping November into the dry or wet period does not significantly change the mean AOT-CO relation for each sensitivity category or the relation of r_e with AOT. Because of the sharp increase of AOT with CO during

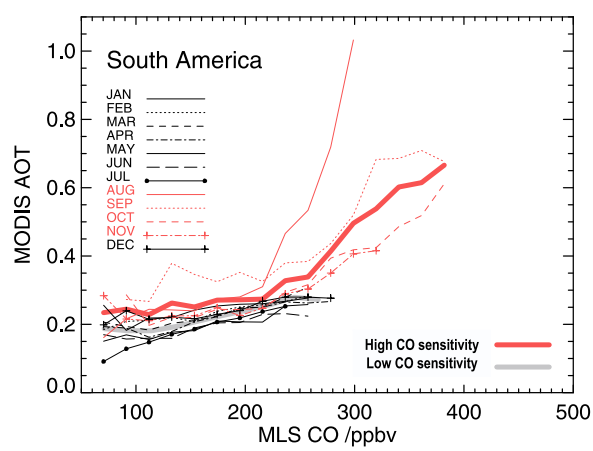

Figure 2. The thin lines are the mean MODIS aerosol optical thickness (AOTs) binned according to the collocated CO values for cloudy (IWC ≥2 mg/m^3) regions in the South America region for all calendar months. The thin red and black lines denote the high CO sensitivity and low CO sensitivity months, respectively (see text for details). The thick red and gray lines represent the averages for all months in the high CO sensitivity and low CO sensitivity periods, respectively.

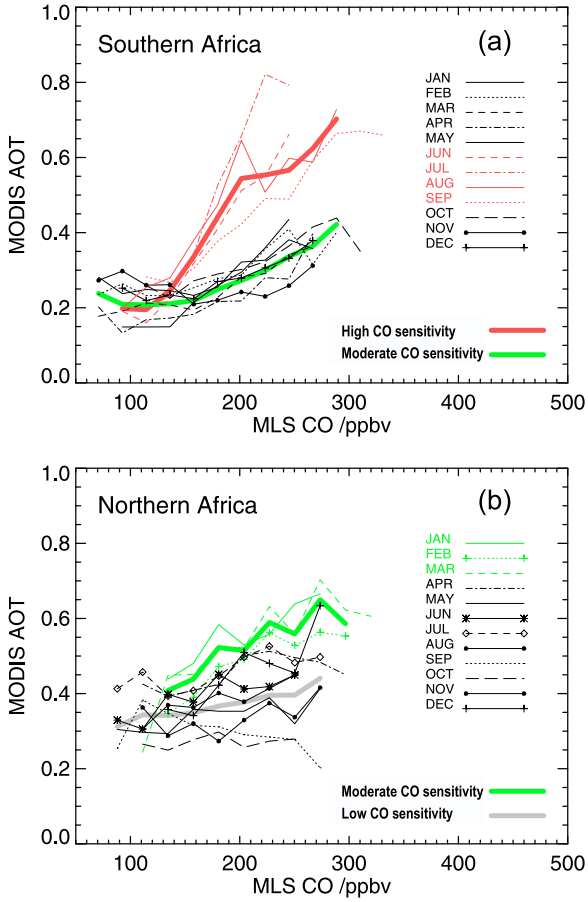

Figure 3. Same as in Figure 2 but for the (a) southern Africa and (b) northern Africa regions. Here the thin green lines are for the individual moderate CO sensitivity months, and the thick green line is the average of the same sensitivity category.

the high CO sensitivity period, CO is a good index of AOT when CO is higher than ~200 ppbv. However, during the low CO sensitivity period, increasing CO is not accompanied by significant increase of AOT. Thus, CO is not a good index of AOT during this period.

3.2. Southern Africa and Northern Africa

[14] Africa is the largest source of biomass burning emissions, where millions of acres of African landscape are burned each year, releasing an order of ~100 Tg/yr of aerosols [e.g., *Formenti et al.*, 2002; *Andreae and Rosenfeld*, 2008]. Africa is characterized by two distinct biomass burning zones: The southern Africa (SAF) burnings are similar to those in SAM, which occur between June and September and generally move from the northeast to southwest of the SAF. The northern Africa (NAF) fires occur primarily in the Sahel and move from the northern to the southern Sahel between November and February [e.g., *Roberts et al.*, 2008]. Fires are not common in the equatorial areas of the "woodland," which is dominated by moist tropical rain forests [e.g., *Bucini and Lambin*, 2002].

[15] Figure 3 shows the AOT-CO relations for SAF and NAF. The SAF burning usually peaks in July, which is reflected by the large slope of the AOT-CO relation during the dry June–September season (Figure 3a). The other months in SAF show a moderate increase of AOT with CO, which we characterize as moderate CO sensitivity, as the AOT differences for the polluted and clean clouds are within 0.1 and 0.2. The NAF fire peaks in January; thus, the largest AOT enhancement in NAF appears in the January–March season (Figure 3b), which also correlates with the CO enhancement. In the other months, AOT increases slowly with increasing CO, so they fall into the low CO sensitivity period.

[16] October and April represent the times of transition between the burnings in SAF and NAF, respectively, when the overall burning is at its weakest due to the transition from dry to wet seasons in the two regions. However, there is a large amount of dust in northern Africa in all months. Unlike biomass burning aerosols, dust particles are not accompanied by CO emissions, which may explain why AOT values are high in NAF but the correlation with CO is low during nonbiomass burning periods (April–December) (Figure 3b).

3.3. South Asia and East Asia

[17] South Asia (SAS) aerosol emissions mostly come from biomass and agriculture burnings (which usually peak in spring) and other anthropogenic sources. East Asia (EAS), which includes many megacities such as Beijing, Shanghai, and Tokyo, is characterized by high population density and heavy anthropogenic emissions from power plants, transportation, infrastructure construction, and other industrial activities. These anthropogenic sources have little seasonal variation. Sulfur emissions from the anthropogenic sources (e.g., fossil fuel combustion) are typically much stronger than that from the biomass burning sources. Both SAS and EAS regions are also influenced by dust storms from the Arabian Peninsula, Taklamakan, and Gobi Deserts, which occur mostly during spring.

[18] In SAS, the AOT-CO relations (Figure 4a) are similar in all months, with AOT increasing with CO moderately throughout the year. Thus, we classify all months in SAS as of moderate CO-sensitivity.

[19] In EAS (Figure 4b), the AOT-CO relations are highly variable. From January to July, dust mixed with sulfate is prevalent. AOT is generally high but does not correlate with CO strongly. From October to December, aerosol stays relatively low. Only during August and September does AOT and CO have an approximate positive relationship. This period is marked as the moderate CO sensitivity period, and the other months fall into the low CO sensitivity period.

3.4. Summary of Regional AOT-CO Relations

[20] As shown in Figures 2–4, the AOT-CO relations can be grouped into three categories.

[21] 1. For high AOT sensitivity to CO, the binned AOT versus CO curve shows a rapid increase of AOT with increasing CO. The AOT in the CO-polluted clouds is more than 0.2 higher than that in the clean clouds. Only two regions during the dry biomass burning season show this high sensitivity, namely, August–November in SAM and June–September in SAF.

[22] 2. For moderate AOT sensitivity to CO, this category appears in most regions with the increase of AOT with CO roughly corresponding to about a 0.1–0.2 AOT difference between the polluted clouds and clean clouds. This includes

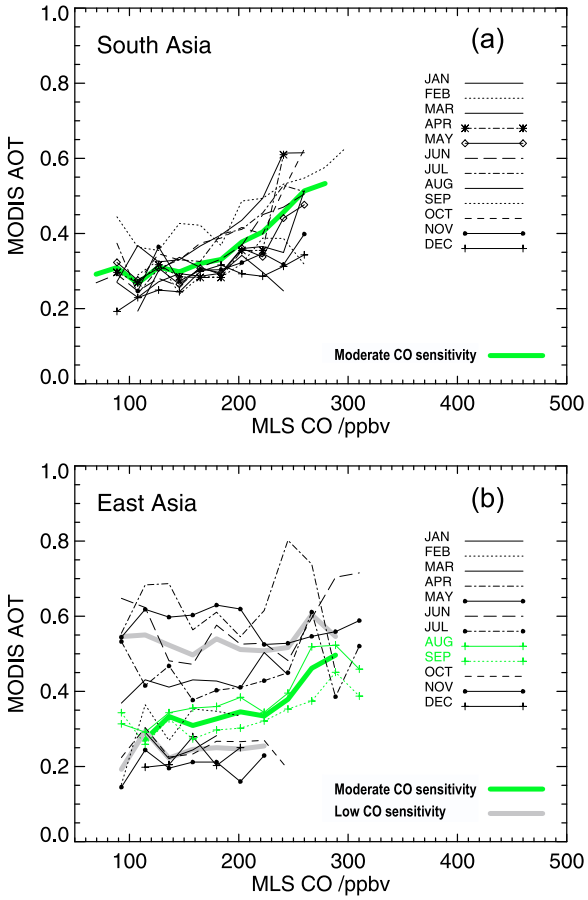

Figure 4. Same as in Figure 3 but for the (a) South Asia and (b) East Asia regions.

the October–May season in SAF, the January–March biomass burning season in NAF, the August–September season in EAS, and all months in SAS which include biomass burning aerosols in spring and anthropogenic aerosols all year around.

[23] 3. For low AOT sensitivity to CO, AOT either comes from dust which does not correlate with CO, or aerosol is washed out by precipitation, while CO is unaffected. This includes the wet rainy season (December–July) in SAM, April–December in NAF, and most months except August–September in EAS.

4. Aerosol Influence on Ice Cloud Particle Size

[24] We now examine the collocated MODIS ice cloud effective radii (r_e) for all five regions for all months, focusing on the differences of r_e between the polluted and clouds at a given IWC. We find that the r_e differences between the polluted clouds and clean clouds are similar within each sensitivity category but distinctly different for different sensitivity categories. Therefore, Figure 5 shows the r_e differences for the polluted and clean clouds grouped by the sensitivity categories for each of the five regions. The high CO sensitivity category exhibits a large reduction of r_e for polluted clouds compared to clean clouds with the same IWC. The r_e reduction for polluted clouds in the moderate CO sensitivity category is evident but smaller than the high CO sensitivity case. For the low CO sensitivity case, the CO-polluted clouds do not show a significantly different r_e from the clean clouds. In this case, the higher CO in the polluted clouds does not correspond to high AOT; thus, it does not indicate the aerosol effects on r_e. Figure 5 suggests that there is indeed a reduction in ice cloud particle size when AOT is enhanced, supporting the notion that aerosol may reduce ice cloud particle size (i.e., the aerosol first indirect effect). Using CO as a proxy for AOT is only valid when AOT has a high to moderate sensitivity to CO. During the periods when AOT has a low sensitivity to CO and CO is a not a good proxy of AOT, we cannot distinguish the particle size differences for CO-polluted clouds and clean clouds.

[25] Despite the conspicuous similarity in r_e relations among the different regions within the same sensitivity category, differences exist for each region in terms of actual r_e differences between the polluted and clean clouds. For the moderate CO sensitivity category, SAF shows a clear-cut difference between the polluted and clean clouds, while NAF and EAS show some overlapping of r_e at the high and low values of IWC. SAS shows a nonoverlapping r_e for the polluted and clean clouds, but the mean r_e for both the polluted and clean clouds are generally larger than that for other regions. For the low CO sensitivity case, NAF and EAS both show some increase in r_e for the polluted clouds when IWC is lower than ~20 mg/m^3. This "anti-Twomey" effect might be significant as suggested by other studies [e.g., *Chylek et al.*, 2006].

[26] Given the complicated AOT-CO-r_e relations for different regions and seasons, it is not obvious if aerosols have a significant effect on ice cloud particle size in the global average. We thus extend our analysis to the global domain (50°S–50°N) and examine the global mean AOT-CO-r_e relations.

5. Global Mean AOT-CO-r_e Relations

[27] Figure 6a shows a scatterplot of AOT versus CO in global convective cloudy regions (when the IWC is ≥2 mg/m^3). All data from August 2004 to July 2008 between 50°S and 50°N are used for this plot. The over-plotted black dots (which are replotted in Figure 6b for clarity) are the mean AOT data binned according to the collocated CO values, and the black line is the linear fit to the binned AOT for the CO ≥100 ppbv regions. The number of data points in each bin is at least 500. Despite large scatter, there is a positive correlation (r = 0.3) between CO and AOT. The AOT is nearly flat and below 0.2 in regions with CO < 100 ppbv. When CO is

Figure 5. MODIS ice cloud effective radius (r_e) binned according to the collocated MLS IWCs for clean and polluted clouds for high, moderate, and low CO sensitivity in each of the five regions as discussed in the text. The error bars in Figures 5 and 6 denote the standard errors ($\sigma/\sqrt{N}$) of the bin average. The polluted clouds are those associated with a high CO loading of 240 ppbv for SAM and SAF and 220 ppbv for other regions; the clean clouds are those associated with low CO of 100 ppbv for SAM and SAF and 110 ppbv for other regions.

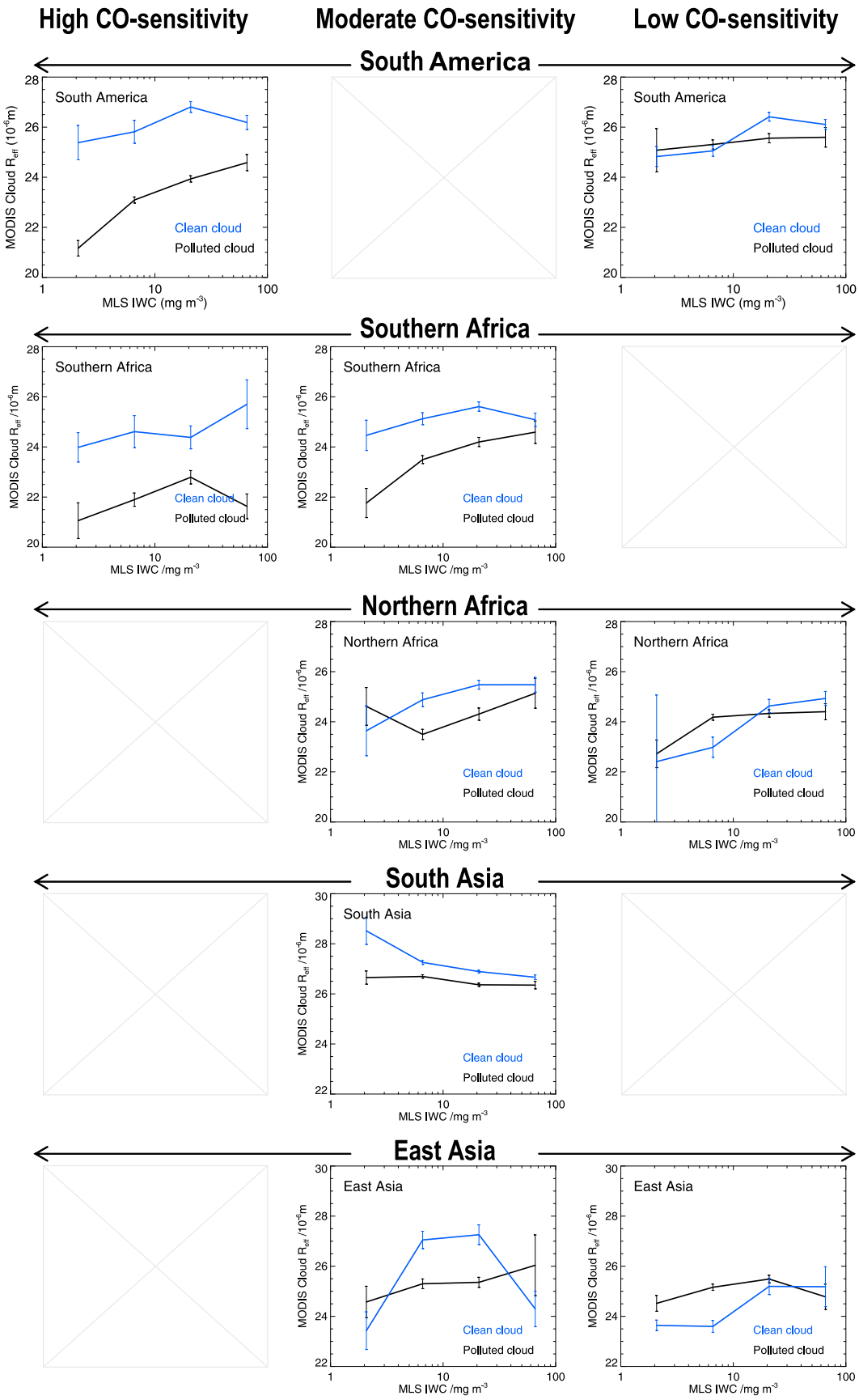
High CO-sensitivity
Moderate CO-sensitivity
Low CO-sensitivity
South America
Southern Africa
Northern Africa
South Asia
East Asia
MODIS Cloud R_{eff} (10^{-6}m)
MLS IWC (mg m^{-3})
Clean cloud
Polluted cloud

Figure 5

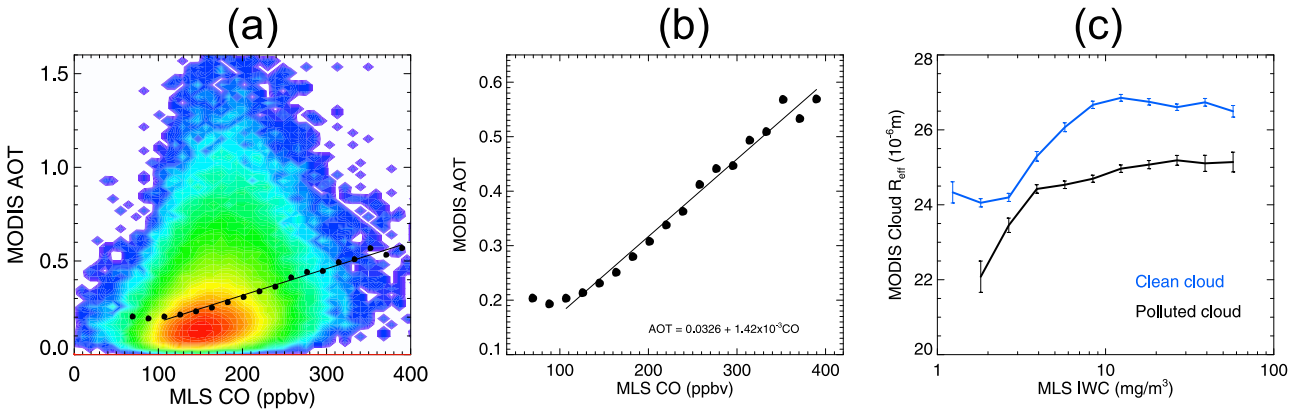

Figure 6. (a) The scatterplot of MODIS AOT versus MLS CO in cloudy regions (IWC is $\geq$2 mg/m^3). The over-plotted black dots are the mean AOT data binned according to the collocated CO values, and the black-line is the linear fit to the binned AOT in the CO $\geq$100 ppbv regions. (b) The black dots from Figure 6a are replotted for clarity. (c) MODIS r_e data binned according to the collocated MLS IWCs for clean (CO $\leq$100 ppbv) and polluted (CO $\geq$240 ppbv) clouds. All data from August 2004 to July 2008 between 50°S and 50°N are used for this plot.

greater than 100 ppbv, the AOT increases linearly at a rate of $\sim$1.4 $\times$ 10^{-3} AOT per ppbv CO mixing ratio. Using CO greater than 240 ppbv as the threshold to separate the polluted and clean clouds, Figure 6c shows that the mean r_e for the global polluted clouds in each IWC bin is smaller than the counterparts for clean clouds over all ranges of IWC.

6. Conclusions and Discussion

[28] This study analyzes the relationship between AOT and CO for a number of regions for all months throughout the year. We characterize the variations of AOT with CO by three categories: high, moderate, and low AOT sensitivity to CO.

[29] For the high and moderate sensitivity periods, AOT increases with CO, with a larger rate during the high sensitivity period. These periods correspond to dry biomass burning seasons in respective regions, such as August–November in SAM, June–September in SAF, and January–March in NAF. Smoke from biomass burnings composes a large part of the aerosols during these periods. The moderate sensitivity periods also include the late monsoon period of August–September in EAS where the anthropogenic aerosol is the main source; October–May in SAF when the biomass burning is weaker; and all year round in SAS, when February–May is the biomass burning season and the rest of year has both anthropogenic aerosols and biomass burning aerosols. The low CO sensitivity periods include the wet rainy season in SAM (December–July), dust-prevailing period (April–December) in NAF, dust storm season (October–April) in EAS and the summer rainy season in EAS (May–July).

[30] The distinctly different AOT sensitivity to CO categories for all regions and seasons is a combined effect of the surface pollution source, convective activity, and large-scale dynamics. With the three level categorization, it is clear where and when CO can be used as a proxy for aerosol loading. CO-polluted clouds (e.g., CO >$\sim$240 ppbv) can be used to indicate aerosol effects only when AOT has high to moderate sensitivity to CO. In this case, CO-polluted clouds have a discernible reduction of cloud particle size compared to clean clouds with the same amount of IWC, indicating the "Twomey-like effect" of aerosol on ice clouds. Meanwhile, the periods with low AOT sensitivity to CO do not show a significant difference in ice cloud particle size for CO-polluted clouds and clean clouds.

[31] The correlations of AOT to CO also appear to be related to aerosol composition. It is known that biomass burning will give rise to both carbonaceous (smoke) and sulfate aerosol as well as CO simultaneously. Thus, the high or moderate CO sensitivity periods are mostly associated with dry biomass burning periods. During wet rainy seasons, precipitation washes out aerosol by wet deposition and scavenging, but CO is retained. Hence, it is not surprising that the wet rainy season in SAM fall into the low CO sensitivity category. Moreover, when dust aerosol dominates the aerosol composition, for example, over NAF and EAS, AOT can be high, but no emission source of CO exists. During these times, AOT and CO do not correlate strongly, and the AOT sensitivity to CO is quite low. For SAS, anthropogenic emissions exist all year around. Aerosol concentrations maintain at a relatively high level, and the positive correlation of AOT and CO is persistent.

[32] Considering the globe as a whole, AOT and CO do have an approximately linear relationship. AOT increases moderately with CO. The CO-polluted clouds tend to have smaller r_e than the clean clouds, consistent with the Twomey-like effect. Such reduction of ice cloud particle size can potentially have important radiative and microphysical effects on the Earth's energy and water cycles.

[33] Our analysis uses 4 years of Aura MLS and Aqua MODIS data and identifies the average relations among AOT, CO, and r_e. Such bulk relations may not apply to individual cases. The ice cloud particle r_e is a function of IWC, pollution loading, temperature, and meteorological conditions. The reduction of r_e for polluted clouds in the global mean does not rule out the possibility that aerosol may increase cloud particle size in particular regions and seasons. Furthermore, it is not clear how the different types of aerosol affect cloud particle size differently based on available data. Nevertheless, the complexity of aerosol effects on clouds,

especially ice clouds, will continue to be analyzed using multiple satellite observations, especially newly released data from the CloudSat and CALIPSO experiments.

[34] **Acknowledgments.** We thank the NASA ROSES05 ACMAP and ROSES06-IDS programs for support. The work was conducted jointly at the Jet Propulsion Laboratory, California Institute of Technology, under contract with NASA; at the National Center for Atmospheric Research, supported by the National Science Foundation; and at the NASA Goddard Space Flight Center.

References

Andreae, M. (1991), Biomass burning: Its history, use and distribution and its impact on environmental quality and global climate, in *Global Biomass Burning: Atmospheric, Climatic and Biospheric Implications*, edited by J. S. Levine, pp. 3–21, MIT Press, Cambridge, Mass.

Andreae, M. O., and D. Rosenfeld (2008), Aerosol-cloud-precipitation interactions, Part I: The nature and sources of cloud-active aerosols, *Earth Sci. Rev.*, *89*, 13–41, doi:10.1016/j.earscirev.2008.03.001.

Bucini, G., and E. F. Lambin (2002), Fire impacts on vegetation in Central Africa: A remote-sensing-based statistical analysis, *Appl. Geogr.*, *22*, 27–48, doi:10.1016/S0143-6228(01)00020-0.

Chylek, P., M. K. Dubey, U. Lohmann, V. Ramanathan, Y. J. Kaufman, G. Lesins, J. Hudson, G. Altmann, and S. Olsen (2006), Aerosol indirect effect over the Indian Ocean, *Geophys. Res. Lett.*, *33*, L06806, doi:10.1029/2005GL025397.

Crutzen, P. J., and M. O. Andreae (1990), Biomass burning in the tropics: Impact on atmospheric chemistry and biogeochemical cycles, *Science*, *250*, 1669–1678, doi:10.1126/science.250.4988.1669.

Denman, K. L., et al. (2007), Couplings between changes in the climate system biogeochemistry, in *Climate Change 2007: The Physical Science Basis. Contribution of Working Group I to the Fourth Assessment Report of the Intergovernmental Panel on Climate Change*, edited by S. Solomon et al., chap. 7, pp. 499–588, Cambridge Univ. Press, New York.

Formenti, P., H. Winklerb, P. Fouriec, S. Pikethd, B. Makgopae, G. Helasa, and M. O. Andreaea (2002), Aerosol optical depth over a remote semi-arid region of South Africa from spectral measurements of the daytime solar extinction and the night-time stellar extinction, *Atmos. Res.*, *62*(1–2), 11–32, doi:10.1016/S0169-8095(02)00021-2.

Fu, R., Y. Hu, J. S. Wright, J. H. Jiang, R. E. Dickinson, M. Chen, M. Filipiak, W. G. Read, J. W. Waters, and D. L. Wu (2006), Short circuit of water vapor and polluted air to the global stratosphere by convective transport over the Tibetan Plateau, *Proc. Natl. Acad. Sci. U. S. A.*, *103*, 5664–5669, doi:10.1073/pnas.0601584103.

Jiang, J. H., N. J. Livesey, H. Su, L. Neary, J. C. McConnell, and N. A. Richards (2007), Connecting surface emissions, convective uplifting, and long-range transport of carbon monoxide in the upper-troposphere: New observations from the Aura Microwave Limb Sounder, *Geophys. Res. Lett.*, *34*, L18812, doi:10.1029/2007GL030638.

Jiang, J. H., H. Su, M. Schoeberl, S. T. Massie, P. Colarco, S. Platnick, and N. Livesey (2008), Clean and polluted clouds: Relationships among pollution, ice clouds, and precipitation in South America, *Geophys. Res. Lett.*, *35*, L14804, doi:10.1029/2008GL034631.

Kim, J., et al. (2004), Aerosol and CO loading in the atmosphere observed by the MODIS and MOPITT: Russian forest fire case, *Proc. SPIE*, *5652*, 263–269, doi:10.1117/12.578903.

Li, Q. B., et al. (2005), Convective outflow of South Asian pollution: A global CTM simulation compared with EOS MLS observations, *Geophys. Res. Lett.*, *32*, L14826, doi:10.1029/2005GL022762.

Lin, J. C., T. Matsui, R. A. Pielke Sr., and C. Kummerow (2006), Effects of biomass-burning-derived aerosols on precipitation and clouds in the Amazon Basin: A satellite empirical study, *J. Geophys. Res.*, *111*, D19204, doi:10.1029/2005JD006884.

Livesey, N. J., et al. (2008), Validation of Aura Microwave Limb Sounder O_3 and CO observations in the upper troposphere and lower stratosphere, *J. Geophys. Res.*, *113*, D15S02, doi:10.1029/2007JD008805.

Lohmann, U., and J. Feichter (2005), Global indirect aerosol effects: A review, *Atmos. Chem. Phys.*, *4*, 7561–7614.

Massie, S. T., J. C. Gille, D. P. Edwards, and S. Nandi (2006), Satellite observations of aerosol and CO over Mexico City, *Atmos. Environ.*, *40*, 6019–6031, doi:10.1016/j.atmosenv.2005.11.065.

Penner, J. E., J. Quaas, T. Storelvmo, T. Takemura, O. Boucher, H. Guo, A. Kirkevåg, J. E. Kristjánsson, and Ø. Seland (2006), Model intercomparison of indirect aerosol effects, *Atmos. Chem. Phys.*, *6*, 3391–3405.

Platnick, S., et al. (2003), The MODIS cloud products: Algorithms and examples from terra, *IEEE Trans. Geosci. Remote Sens.*, *41*, 459–473, doi:10.1109/TGRS.2002.808301.

Remer, L. A., et al. (2005), The MODIS aerosol algorithm, products and validation, *J. Atmos. Sci.*, *62*, 947–973, doi:10.1175/JAS3385.1.

Roberts, G., M. J. Wooster, and E. Lagoudakis (2008), Annual and diurnal African biomassburning temporal dynamics, *Biogeosciences Discuss.*, *5*, 3623–3663.

Schoeberl, M. R., B. N. Duncan, A. R. Douglass, J. Waters, N. Livesey, W. Read, and M. Filipiak (2006), The carbon monoxide tape recorder, *Geophys. Res. Lett.*, *33*, L12811, doi:10.1029/2006GL026178.

Sherwood, S. (2002), Aerosols and ice particle size in tropical cumulonimbus, *J. Clim.*, *15*, 1051–1063, doi:10.1175/1520-0442(2002)015<1051:AAIPSI>2.0.CO;2.

Wu, D. L., J. H. Jiang, W. G. Read, R. T. Austin, C. P. Davis, A. Lambert, G. L. Stephens, D. G. Vane, and J. W. Waters (2008), Validation of the Aura MLS Cloud Ice Water Content Measurements, *J. Geophys. Res.*, *113*, D15S10, doi:10.1029/2007JD008931.

P. R. Colarco, S. Platnick, and M. R. Schoeberl, NASA Goddard Space Flight Center, Code 916, Greenbelt, MD 20771, USA.

J. H. Jiang and H. Su, Jet Propulsion Laboratory, California Institute of Technology, Mail Stop 183-701, 4800 Oak Grove Drive, Pasadena, CA 91109-8099, USA. (jonathan.h.jiang@jpl.nasa.gov)

S. T. Massie, National Center for Atmospheric Research, P.O. Box 3000, Boulder, CO 80307, USA.